Inorganic Chemistry

Article

pubs.acs.org/IC

Nanostructures in Te/Sb/Ge/Ag (TAGS) Thermoelectric Materials Induced by Phase Transitions Associated with Vacancy Ordering

Thorsten Schröder,[†] Tobias Rosenthal,[†] Nadja Giesbrecht,[†] Markus Nentwig,[†] Stefan Maier,[†] Heng Wang,[‡] G. Jeffrey Snyder,[‡] and Oliver Oeckler*[,§]

[†]Department of Chemistry, University of Munich (LMU), Butenandtstr. 5-13 (D), 81377 Munich, Germany

[‡]Materials Science, California Institute of Technology, 1200 E. California Boulevard., Pasadena, California 91125, United States

[§]Faculty of Chemistry and Mineralogy, IMKM, Leipzig University, Scharnhorststr. 20, 04275 Leipzig, Germany

Supporting Information

ABSTRACT: Te/Sb/Ge/Ag (TAGS) materials with rather high concentrations of cation vacancies exhibit improved thermoelectric properties as compared to corresponding conventional TAGS (with constant Ag/Sb ratio of 1) due to a significant reduction of the lattice thermal conductivity. There are different vacancy ordering possibilities depending on the vacancy concentration and the history of heat treatment of the samples. In contrast to the average α-GeTe-type structure of TAGS materials with cation vacancy concentrations <~3%, quenched compounds like $Ge_{0.53}Ag_{0.13}Sb_{0.27}\square_{0.07}Te_1$ and $Ge_{0.61}Ag_{0.11}Sb_{0.22}\square_{0.06}Te_1$ exhibit "parquet-like" multidomain nanostructures with finite intersecting vacancy layers. These are perpendicular to the pseudocubic ⟨111⟩ directions but not equidistantly spaced, comparable to the nanostructures of compounds $(GeTe)_nSb_2Te_3$. Upon heating, the nanostructures transform into long-periodically ordered trigonal phases with parallel van der Waals gaps. These phases are slightly affected by stacking disorder but distinctly different from the α-GeTe-type structure reported for conventional TAGS materials. Deviations from this structure type are evident only from HRTEM images along certain directions or very weak intensities in diffraction patterns. At temperatures above ~400 °C, a rock-salt-type high-temperature phase with statistically disordered cation vacancies is formed. Upon cooling, the long-periodically trigonal phases are reformed at the same temperature. Quenched nanostructured $Ge_{0.53}Ag_{0.13}Sb_{0.27}\square_{0.07}Te_1$ and $Ge_{0.61}Ag_{0.11}Sb_{0.22}\square_{0.06}Te_1$ exhibit ZT values as high as 1.3 and 0.8, respectively, at 160 °C, which is far below the phase transition temperatures. After heat treatment, i.e., without pronounced nanostructure and when only reversible phase transitions occur, the ZT values of $Ge_{0.53}Ag_{0.13}Sb_{0.27}\square_{0.07}Te_1$ and $Ge_{0.61}Ag_{0.11}Sb_{0.22}\square_{0.06}Te_1$ with extended van der Waals gaps amount to 1.6 at 360 °C and 1.4 at 410 °C, respectively, which is at the top end of the range of high-performance TAGS materials.

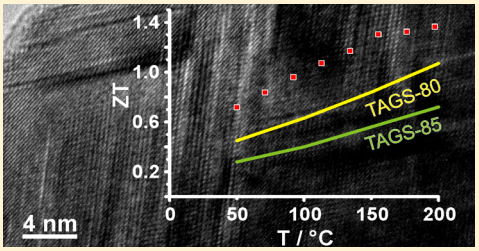

INTRODUCTION

Facing the current energy problems, many ways of increasing the efficiency of energy transformation processes have been evaluated, among them the interconversion of heat and electrical energy by thermoelectric materials. Their efficiency is characterized by the dimensionless figure of merit $ZT = S^2\sigma T/\kappa$ (with the Seebeck coefficient S, the electrical conductivity σ, the temperature T, and the thermal conductivity κ). At moderately high temperatures between 150 and 600 °C, chalcogenides with high ZT values are the materials of choice.[1] Many different materials, e.g., tellurides with rock-salt-type structure like $AgSbTe_2$[2,3] or $AgIn_xSb_{1-x}Te_2$[4,5] as well as heterogeneous $(PbTe)_mAgSbTe_2$ (LAST)[6] materials were recently investigated, along with chalcogenides derived from the sphalerite structure type, such as $Cu_2Zn_{1-x}Fe_xGeSe_4$,[7] $CuGaTe_2$,[8,9] or $CuInTe_2$.[10] The so-called TAGS-x materials $(GeTe)_x(AgSbTe_2)_{100-x}$, which crystallize in the α-GeTe structure type at ambient conditions and exhibit rock-salt-type high-temperature (HT) phases, represent some of the classical and best characterized thermoelectric materials with ZT values above 1.[11−14] They can be understood as quasibinary solid solutions between $AgSbTe_2$ and GeTe[15,16] and reach ZT values of up to 1.7 at 500 °C.[17] In order to optimize the thermoelectric properties of TAGS, many different substitution variants were investigated, e.g., Ge^{2+} was replaced by Sn^{2+} in $(SnTe)_xAgSbTe_2$,[18] Ag^+ by Li^+ in $(GeTe)_x(LiSbTe_2)_2$,[19] and Sb^{3+} by In^{3+} in $(GeTe)_xAgInTe_2$ and $(GeTe)_xAgIn_{0.5}Sb_{0.5}Te_2$.[20] Even doping with rare earth metals was considered.[21,22] Extending the compositional range of TAGS materials beyond pseudobinary solid solutions $(GeTe)_x(AgSbTe_2)_{100-x}$ leads to compounds $(GeTe)_x[(Ag_2Te)_y(Sb_2Te_3)_{1-y}]_{100-x}$,[23] where the Ag/Sb ratio is variable. This approach leads to improved thermoelectric properties in high-performance TAGS materials like $(GeTe)_{85}(Ag_ySbTe_{y/2+1.5})_{15}$, where the thermal conductivity is reduced without significantly affecting the electrical conductivity[24] and the power factor is increased due to an optimized charge carrier concentration without decreasing the

Received: May 5, 2014
Published: July 7, 2014

   dx.doi.org/10.1021/ic5010243 | Inorg. Chem. 2014, 53, 7722−7729

carrier mobility.[25,26] This extension involves cation vacancies for all values of $y < 1$, because y atoms of Ag but only $y/2$ atoms of Te are removed as compared to TAGS-x, which results in a larger number of anions than cations. The impact and the ordering possibilities of cation vacancies have not been taken into consideration so far in the literature. In compounds $(GeTe)_nSb_2Te_3$ (n = 12, 19), which correspond to TAGS $(GeTe)_x(Ag_ySbTe_{y/2+1.5})_{100-x}$ with y = 0 and consequently exhibit maximal cation vacancy concentrations, different cation vacancy ordering motifs were described, depending on the composition (n) and the thermal treatment.[27] Upon quenching, these compounds $(GeTe)_nSb_2Te_3$ form metastable pseudocubic phases in contrast to the α-GeTe-type structure of vacancy-free TAGS, whose cubic HT phase cannot be retained at ambient temperature by quenching as the phase transition is displacive. The reason for the formation of such pseudocubic structures lies in their "parquet-like" nanoscale domain structures produced by short-range vacancy ordering in layers perpendicular to the cubic ⟨111⟩ directions.[28] These layers are not equidistantly spaced, which results in diffuse streaks along ⟨111⟩* in diffraction patterns. Upon heating, the atoms next to the vacancy layers rearrange to form extended parallel van der Waals gaps. Stacking disorder is typical and results in an α-Hg-type average structure. At higher temperatures (typically above ~500 °C), a rock-salt-type HT phase with randomly disordered cation vacancies is formed. If this is slowly cooled, the above-mentioned trigonal phase is formed.

The formation of comparable "parquet-like" nanostructures can be expected to be beneficial for the thermoelectric properties of high-performance TAGS materials, too, although the existence of multiple phase transitions might be a drawback for the thermal cycling behavior of these materials. In the present work, the effects of the cation vacancy concentration on the structure, stability, and properties of TAGS materials with cation vacancies are studied.

EXPERIMENTAL SECTION

Synthesis. Samples with the nominal compositions $Ge_{0.53}Ag_{0.13}Sb_{0.27}Te_1$, $Ge_{0.61}Ag_{0.11}Sb_{0.22}Te_1$, and $Ge_{0.77}Ag_{0.07}Sb_{0.13}Te_1$ were synthesized by melting stoichiometric mixtures (typically 2.0 g) of the pure elements (silver 99.9999%, Alfa Aesar; germanium 99.999%, Sigma-Aldrich; antimony 99.9999%, Smart Elements; tellurium 99.999%, Alfa Aesar) at 900 °C under Ar atmosphere in silica glass ampules for 1 day and subsequently quenching the ampules to room temperature (RT) by removing from the furnace. The samples were then annealed at 500 °C for 3 days and again quenched to RT in the same fashion. Samples for thermoelectric characterization were synthesized in the same manner; however, larger ampules (diameter 1.2 cm) with a flat bottom were used to quench the melts in order to obtain ingots with dimensions as required for the measurements. The disc-shaped ingots were subsequently ground down until the round faces were parallel and finally polished. For these discs, homogeneity and absence of side phases were verified in the same manner as for all samples; the synthesis is well reproducible.

Diffraction Methods. A Huber G670 Guinier camera equipped with a fixed imaging plate and integrated read-out system using Cu Kα1 radiation (Ge(111) monochromator, λ = 1.540 51 Å) was used for the collection of powder X-ray diffraction (PXRD) patterns of representative parts of the crushed samples, which were fixed between two Mylar foils using vacuum grease. A STOE Stadi P powder diffractometer equipped with an imaging-plate detector system using Mo Kα1 radiation (Ge(111) monochromator, λ = 0.710 93 Å) in a modified Debye–Scherrer geometry equipped with a graphite furnace was used for the collection of temperature-dependent powder diffraction patterns from RT to 600 °C with a heating rate of 10 K/min and from 600 °C back to RT with cooling rate of 5 K/min (faster cooling is impossible with the setup used). For these temperature-dependent measurements, powdered samples were filled into silica glass capillaries (0.3 mm diameter), which were then sealed with vacuum grease under argon atmosphere. Rietveld refinements were carried out using the program TOPAS;[29] phase homogeneity and the temperature-dependent powder diffraction patterns were evaluated using WINXPOW.[30]

Electron Microscopy, Diffraction, and X-ray Spectroscopy. X-ray spectra of representative parts of the samples were recorded with an energy dispersive X-ray (EDX) detector (model 7418, Oxford Instruments, Great Britain) mounted on a JSM-6500F (Jeol) scanning electron microscope (SEM). The results of 6 point analyses were averaged. Detailed results are given in Table S1 in the Supporting Information.

Finely ground samples were dispersed in ethanol and distributed on copper grids coated with holey carbon film (S166-2, Plano GmbH, Germany) for high-resolution transmission electron microscopy (HRTEM). The copper grids were subsequently fixed on a double-tilt holder and investigated in a Titan 80-300 (FEI) equipped with a TEM TOPS 30 EDX spectrometer (EDAX, Germany) and a field-emission gun operated at 300 kV. Selected-area electron diffraction (SAED) patterns and HRTEM images were recorded using an UltraScan 1000 camera (Gatan, resolution 2k × 2k). The Digital Micrograph[31] and EMS software packages[32] were used for HRTEM and SAED data evaluation; EDX data were evaluated with ES Vision.[33]

Thermoelectric Characterization. For the characterization of the thermoelectric properties of $Ge_{0.53}Ag_{0.13}Sb_{0.27}\square_{0.07}Te_1$ and $Ge_{0.61}Ag_{0.11}Sb_{0.22}\square_{0.06}Te_1$ between 50 and 450 °C, three samples of each composition were synthesized as irreversible phase transitions (see thermal behavior section) were expected, which affect the transport properties. In order to obtain reliable ZT values for quenched samples at low temperatures, i.e., where the nanostructure is inert, each property was measured using a sample that had not undergone previous heating cycles. All analytical methods applied did not indicate any differences between samples with the same composition and thermal treatment. The electrical conductivity σ was measured in-plane using pressure-assisted Nb contacts in an in-house built facility at Caltech[34] using the van der Pauw method[35] (heating rate 150 K/h, measurement in 50 K steps). An LFA457 MicroFlash (Netzsch, Germany) laser flash system was used for the out-of-plane measurement of the thermal diffusivity D_{th}. The thermal conductivity was calculated as $\kappa = D_{th}C_p\rho$ where C_p is the heat capacity calculated according to the Dulong–Petit approximation, which has turned out to be valid for telluride thermoelectric materials in the temperature range investigated; in such cases experimental values affected by baseline shifts may lead to a larger uncertainty than the theoretical values,[36] i.e., 0.226 J/gK for $Ge_{0.53}Ag_{0.13}Sb_{0.27}\square_{0.07}Te_1$ and 0.230 J/gK for $Ge_{0.61}Ag_{0.11}Sb_{0.22}\square_{0.06}Te_1$ (ρ = density determined by weighing the sample and measuring its dimensions). The Seebeck coefficient S was determined out-of-plane using Chromel-Nb thermocouples in steps of 61 K at a heating rate of 150 K/h and a temperature oscillation rate of ±7.5 K.[37] The combined uncertainty of the measurements is ca. 20% for the ZT value.

RESULTS AND DISCUSSION

Overview and Sample Characterization. In principle, there are three ways (and combinations of them) of introducing cation vacancies (□) in TAGS materials without affecting the overall charge neutrality: (1) the exchange of 1 Ag^+ by 0.5 Ge^{2+} and 0.5 □, (2) the exchange of 1 Ag^+ by $^1/_3$ Sb^{3+} and $^2/_3$ □, and (3) the exchange of 1 Ge^{2+} by $^2/_3$ Sb^{3+} and $^1/_3$ □. These different possibilities make it difficult to maintain the widespread TAGS-x nomenclature (with x given by $(GeTe)_x(AgSbTe_2)_{100-x}$). For example, $Ge_{0.53}Ag_{0.13}Sb_{0.27}\square_{0.07}Te_1$ may be written as $Ge_4AgSb_2Te_{7.5}$, which on one hand could be understood as a variant of TAGS-80 = $(GeTe)_{80}(AgSbTe_2)_{20}$ = $(GeTe)_4AgSbTe_2$ = $Ge_4AgSbTe_6$ with additional 0.5 Sb_2Te_3 per formula unit, or

dx.doi.org/10.1021/ic5010243 | Inorg. Chem. 2014, 53, 7722–7729

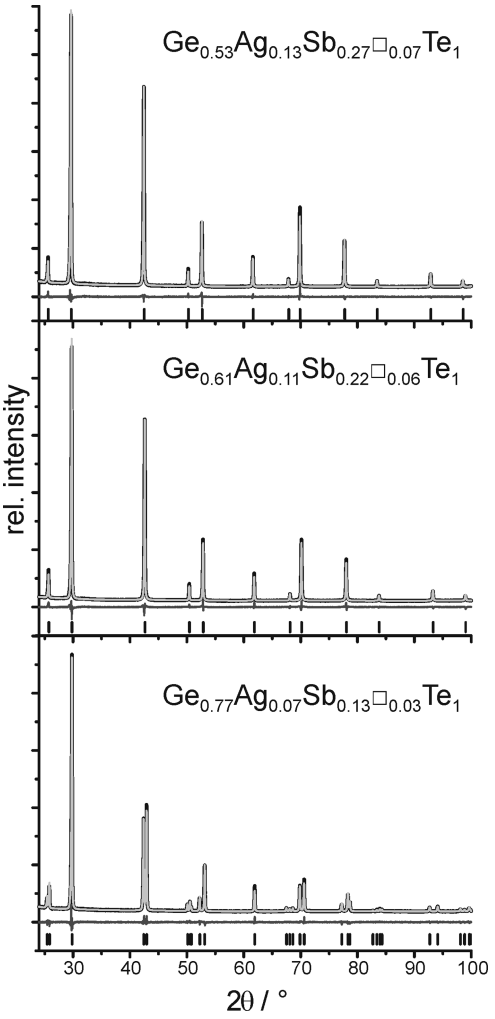

Figure 1. Experimental (black) and calculated (light gray) powder diffraction patterns according to the Rietveld refinement of $Ge_{0.53}Ag_{0.13}Sb_{0.27}\square_{0.07}Te_1$, $Ge_{0.61}Ag_{0.11}Sb_{0.22}\square_{0.06}Te_1$, and $Ge_{0.77}Ag_{0.07}Sb_{0.13}\square_{0.03}Te_1$ (top to bottom), with difference plots (black, below the profiles) and peak positions (black lines).

on the other hand can also be viewed as TAGS-85 = $(GeTe)_{85}(AgSbTe_2)_{15} \approx (GeTe)_{5.5}AgSbTe_2 = Ge_{5.5}AgSbTe_{7.5}$ with 1.5 Ge^{2+} being replaced by 1 Sb^{3+}. Therefore, the comparison of vacancy-containing compounds with conventional TAGS-*x* is not unequivocal. Similarly, a given vacancy concentration is not sufficient to characterize modified TAGS materials, because there are different element combinations that correspond to the same amount of cation vacancies. For the sake of clarity, we use normalized formulas that immediately show the vacancy concentration as a consequence of the site occupancies in possibly distorted rock-salt-type structures that are characteristic for all compounds discussed here: they exhibit just one cation and one anion position. For example, $Ge_4AgSb_2Te_{7.5}$ is written as $Ge_{0.53}Ag_{0.13}Sb_{0.27}\square_{0.07}Te_1$.

Many experiments have shown that all of these variations lead to single-phase samples as long as charge neutrality is not violated. If the anion and cation charges are not balanced, binary side phases or remaining elemental Ge or Te are observed. All samples discussed in this Article are single-phase as shown by Rietveld refinements (cf., next section); typically the weight of the ingot differs from that of the mixture of starting materials by less than 1%. The composition and homogeneity are further confirmed by SEM-EDX results (cf. Table S1 in the Supporting Information).

Crystal Structures of the Quenched Compounds. All reflections in the PXRD patterns of $Ge_{0.53}Ag_{0.13}Sb_{0.27}\square_{0.07}Te_1$ and $Ge_{0.61}Ag_{0.11}Sb_{0.22}\square_{0.06}Te_1$ can be indexed assuming the rock-salt-type's cubic metrics. In contrast, reflection splitting indicates that $Ge_{0.77}Ag_{0.07}Sb_{0.13}\square_{0.03}Te_1$ is rhombohedral; the unit cell corresponds to the α-GeTe type. The latter compound is discussed in order to demonstrate the influence of the vacancy concentration on the average structure in the case of high Ge contents; however, it was not further characterized as its expected low Seebeck coefficient (already lowered for $Ge_{0.53}Ag_{0.13}Sb_{0.27}\square_{0.07}Te_1$ compared to $Ge_{0.61}Ag_{0.11}Sb_{0.22}\square_{0.06}Te_1$; see Thermoelectric Properties section) precludes promising thermoelectric properties. Rietveld refinements for $Ge_{0.53}Ag_{0.13}Sb_{0.27}\square_{0.07}Te_1$ and $Ge_{0.61}Ag_{0.11}Sb_{0.22}\square_{0.06}Te_1$ confirm the presence of rock-salt-type average structures. In order to exclude rhombohedral

Table 1. Crystal Data and Results of the Rietveld Refinement of $Ge_{0.53}Ag_{0.13}Sb_{0.27}\square_{0.07}Te_1$, $Ge_{0.61}Ag_{0.11}Sb_{0.22}\square_{0.06}Te_1$, and $Ge_{0.77}Ag_{0.07}Sb_{0.13}\square_{0.03}Te_1$

	$Ge_{0.53}Ag_{0.13}Sb_{0.27}\square_{0.07}Te_1$	$Ge_{0.61}Ag_{0.11}Sb_{0.22}\square_{0.06}Te_1$	$Ge_{0.77}Ag_{0.07}Sb_{0.13}\square_{0.03}Te_1$
molar mass (of asymmetric unit)/g mol^{-1}	213.16	210.97	206.71
cryst system/space group	cubic/$Fm\bar{3}m$ (No. 225)	cubic/$Fm\bar{3}m$ (No. 225)	trigonal/$R3m$ (No. 160)
Z	4	4	3
$F(000)$	355.7	352.4	259.4
lattice params/Å	6.011 75(2)	5.992 53(2)	a = 4.209 35(2), c = 10.4922(1)
cell volume/Å^3	217.272(2)	215.194(2)	161.001(3)
density (X-ray)/g cm^{-3}	6.52	6.51	6.40
abs coeff/mm^{-1}	147.2	143.9	134.8
radiation	Cu Kα1 (λ = 1.540 596 Å)	Cu Kα1 (λ = 1.540 596 Å)	Cu Kα1 (λ = 1.540 596 Å)
2θ range/deg	24–100	24–100	24–100
no. data points	15 201	15 201	15 201
no. reflns	13	13	31
constraints	2	2	4
refined params/thereof background	22/12	22/12	27/12
R_p/R_{wp}	0.0173/0.0275	0.0254/0.0371	0.0181/0.0280
R_{Bragg}	0.0139	0.0182	0.0147
GOF	0.997	1.430	0.947

dx.doi.org/10.1021/ic5010243 | Inorg. Chem. 2014, 53, 7722–7729

Table 2. Atom Positions, Occupancy Factors (sof), and Displacement Parameters (B_{iso} in Å^2) of $Ge_{0.53}Ag_{0.13}Sb_{0.27}\square_{0.07}Te_1$, $Ge_{0.61}Ag_{0.11}Sb_{0.22}\square_{0.06}Te_1$, and $Ge_{0.77}Ag_{0.07}Sb_{0.13}\square_{0.03}Te_1$

sample	atom	*x y z*	sof	B_{iso}
$Ge_{0.53}Ag_{0.13}Sb_{0.27}\square_{0.07}Te_1$	Ge/Ag/Sb	0 0 0	0.533/0.133/0.267	2.66(1)
	Te	0.5 0.5 0.5	1	0.96(1)
$Ge_{0.61}Ag_{0.11}Sb_{0.22}\square_{0.06}Te_1$	Ge/Ag/Sb	0 0 0	0.611/0.111/0.222	2.76(2)
	Te	0.5 0.5 0.5	1	1.05(1)
$Ge_{0.77}Ag_{0.07}Sb_{0.13}\square_{0.03}Te_1$	Ge/Ag/Sb	0 0 0.4834(2)	0.767/0.067/0.133	2.12(3)
	Te	0 0 0	1	1.35(2)

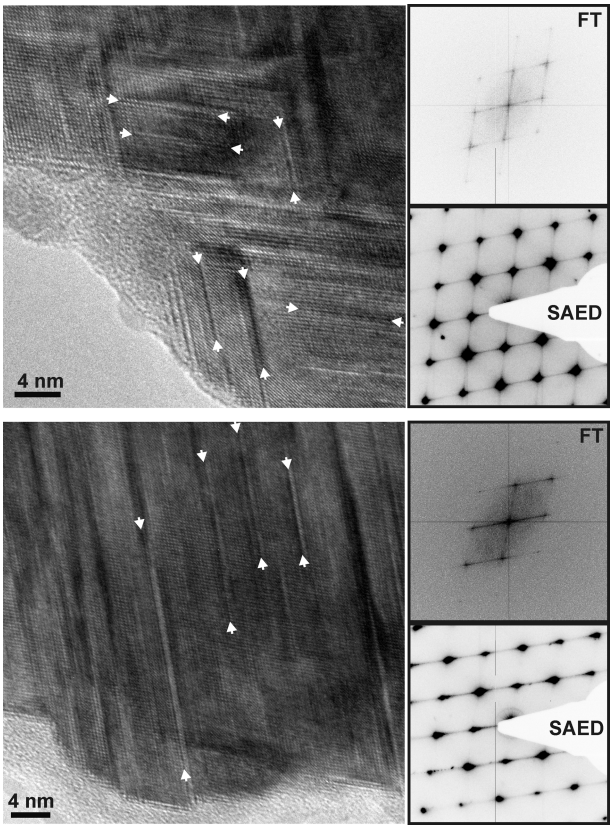

Figure 2. HRTEM images of quenched $Ge_{0.61}Ag_{0.11}Sb_{0.22}\square_{0.06}Te_1$ (top) and a different area of the same crystallite after prolonged exposure to the electron beam (bottom) with the corresponding Fourier transforms (FT) and SAED patterns of the crystallite (all along the zone axis [110] with respect to cubic indexing). Some selected vacancy layers are highlighted by white arrows, and their arrangement is indicated.

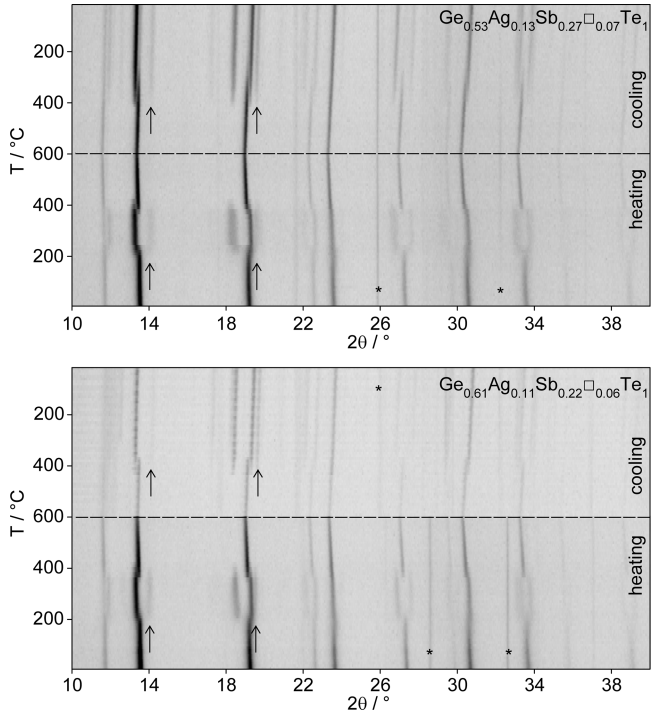

Figure 3. Temperature-dependent PXRD patterns of $Ge_{0.53}Ag_{0.13}Sb_{0.27}\square_{0.07}Te_1$ (top) and $Ge_{0.61}Ag_{0.11}Sb_{0.22}\square_{0.06}Te_1$ (bottom, note that different contrast of the cooling section is due to the use of another measurement, asterisks mark the positions of reflections caused by the furnace). Two of the strongest additional reflections that indicate the formation of a long-periodically ordered trigonal phase are marked with arrows; the dashed horizontal line marks the highest temperature.

structures with pseudocubic metrics, which have been reported in the Ag/Ge/In/Sb/Te system,[20] various test refinements were performed. Layer formation like in α-GeTe reduces the symmetry from $Fm\bar{3}m$ to $R3m$. A measure of this layer formation is the z parameter of the cations which is 0.5 in the trigonal setting of the cubic unit cell. No significant deviations from this value were detected. In the final refinements, common atom coordinates and displacement parameters were refined for all cations. Cation site occupancies were taken from the nominal composition and not refined; tentative refinements did not indicate significant changes. The Te anion position was assumed as completely occupied with an independent displacement parameter. For the refinements in the space group $R3m$, preferred orientation was considered as a flat sample holder was used (4th order spherical harmonics with 3 parameters). The profile fits are depicted in Figure 1; the results of the refinement and the atomic parameters are given in Tables 1 and 2, respectively. Further details of the crystal structure investigations may be obtained from Fachinformationszentrum Karlsruhe, 76344 Eggenstein-Leopoldshafen, Germany (fax (+49)7247-808-666; e-mail crysdata@fiz-karlsruhe.de, http://www.fiz-karlsruhe.de/request_for_deposited_data.html) on quoting the depository numbers CSD 427403, 427405, and 427404 for $Ge_{0.53}Ag_{0.13}Sb_{0.27}\square_{0.07}Te_1$, $Ge_{0.61}Ag_{0.11}Sb_{0.22}\square_{0.06}Te_1$, and $Ge_{0.77}Ag_{0.07}Sb_{0.13}\square_{0.03}Te_1$, respectively.

The rock-salt-type average structure of $Ge_{0.53}Ag_{0.13}Sb_{0.27}\square_{0.07}Te_1$ and $Ge_{0.61}Ag_{0.11}Sb_{0.22}\square_{0.06}Te_1$ is an uncommon observation for TAGS materials, because usually it is not possible to quench their cubic HT phase due to the displacive character of the phase transition. This hints at the crucial role of cation vacancy ordering in the compounds investigated (see below). With increasing GeTe content, the lattice parameter decreases. In addition to the metrics indicated by reflection splitting, the α-GeTe type structure of

dx.doi.org/10.1021/ic5010243 | Inorg. Chem. 2014, 53, 7722−7729

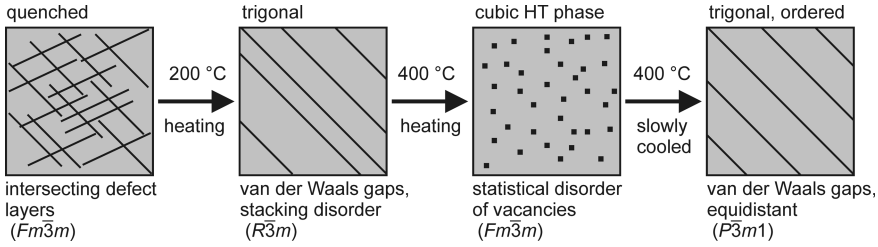

Figure 4. Schematic illustration of the rearrangement of the vacancies during heating and cooling.

$Ge_{0.77}Ag_{0.07}Sb_{0.13}\square_{0.03}Te_1$ is corroborated by the cation z parameter of 0.4834(2) which indicates pronounced layer formation.

Transmission Electron Microscopy. HRTEM investigations (cf., Figure 2) reveal the ordering of cation defects in a sample of $Ge_{0.61}Ag_{0.11}Sb_{0.22}\square_{0.06}Te_1$, which was quenched after being annealed in the stability range of the cubic HT phase (see section below). The nanostructure is comparable to the one observed for Ag-free $(GeTe)_nSb_2Te_3$ thermoelectric materials.[28] The average lateral extension of the defect layers (measured in HRTEM images) is 9(2) nm in good agreement with the lateral extension of 11(3) nm observed for $(GeTe)_7Sb_2Te_3$, which exhibits a similar cation vacancy concentration.[38] The defect layers in both compounds are perpendicular to the cubic ⟨111⟩ directions; they intersect and thereby form a "parquet-like" multidomain nanostructure (cf. Figure 2, top). The observation that the defect layers form van der Waals gaps at higher temperatures (see next section) and the fact that the average structure of the investigated compound is cubic ($Fm\bar{3}m$) corroborates that the planar defects correspond to cation vacancy layers as opposed to twin boundaries in conventional trigonal TAGS materials (corresponding to the symmetry reduction from $Fm\bar{3}m$ to $R3m$ upon cooling the HT phase). The average distance between the vacancy layers is 4(1) nm; however, they are not equidistant as corroborated by diffuse streaks that interconnect Bragg reflections along ⟨111⟩* in the SAED patterns taken along the [110] zone axis and the corresponding Fourier transforms of HRTEM images. This nanostructure is not limited to thin fringes of the particles, but extends over the whole crystallites (cf., Figure S2, bottom, in the Supporting Information). Due to their special orientation, defect layers and corresponding diffuse intensities cannot be observed in HRTEM images or SAED patterns along most zone axes (e.g., [100], cf., Figure S2, top, in Supporting Information). The same type of nanostructure is also observed in quenched $Ge_{0.53}Ag_{0.13}Sb_{0.27}\square_{0.07}Te_1$ (cf. Figure S1 in Supporting Information).

Larger areas with parallel defect layers (lateral extension >25 nm), which are more regularly spaced (average spacing: 3.5(5) nm) and correspond to extended van der Waals gaps, were observed after prolonged exposure to the electron beam (cf. Figure 2, bottom). This indicates a tendency toward long-range order comparable to that in annealed samples of $(GeTe)_nSb_2Te_3$.[28]

Stability Ranges and Phase Transitions. Temperature-dependent PXRD patterns of quenched $Ge_{0.53}Ag_{0.13}Sb_{0.27}\square_{0.07}Te_1$ and $Ge_{0.61}Ag_{0.11}Sb_{0.22}\square_{0.06}Te_1$ (see Figure 3) show that upon heating in both compounds the pseudocubic phase (with "parquet-like" multidomain nanostructure) transforms to a trigonal, long-periodically ordered phase at ca. 200 °C. This is indicated by reflection splitting and additional weak reflections, e.g., at 2θ = 14° and 20°. During heating, these reflections are rather broad, which indicates severe stacking disorder and impedes the assignment of a distinct structure type. At ca. 400 °C, both compounds form their rock-salt-type HT phases with statistically disordered cation vacancies. Upon cooling, they retransform to the trigonal long-periodically ordered structures. A schematic illustration of the rearrangements of the vacancy layers is depicted in Figure 4. Owing to the slow cooling process, the weak reflections of the trigonal phase are sharper than they were during the heating process. Therefore, the $Ge_5As_2Te_8$ structure type with a 15P stacking sequence (space group $P\bar{3}m1$ (No. 164), a = 4.2136(3) Å; c = 27.711(4) Å) can be assigned for $Ge_{0.53}Ag_{0.13}Sb_{0.27}\square_{0.07}Te_1$ (cf., Figure S3 and Table S2 in the Supporting Information). This structure can be understood as a sequence of slightly distorted 15-layer slabs cut out of the rock-salt-type structure, which are terminated by Te atom layers and separated by van der Waals gaps (cf., Figure S4 in the Supporting Information). Around the latter, the Te−Te stacking sequence corresponds to a hexagonal ABAB one. This rearrangement of cation vacancies corresponds to a reconstructive phase transition. For such layered phases, the number of layers between the van der Waals gaps can be estimated from the vacancy concentration as detailed in the literature.[39] In the case of $Ge_{0.53}Ag_{0.13}Sb_{0.27}\square_{0.07}Te_1$ the expected number of layers (1/0.067 = 15) corresponds exactly to the observed one.

Thermoelectric Properties of $Ge_{0.53}Ag_{0.13}Sb_{0.27}\square_{0.07}Te_1$ and $Ge_{0.61}Ag_{0.11}Sb_{0.22}\square_{0.06}Te_1$. The thermoelectric properties of nanostructured $Ge_{0.53}Ag_{0.13}Sb_{0.27}\square_{0.07}Te_1$ and $Ge_{0.61}Ag_{0.11}Sb_{0.22}\square_{0.06}Te_1$ (cf. Figure 5) as measured at the beginning of the first heating cycle change after heating over 200 °C as expected by the phase transitions as described above, when the finite intersecting defect layers become extended and parallel. As the structural changes during the first heating measurement between 200 and 450 °C can be viewed as a slow ongoing ordering process, the measured properties in this range shall not be discussed as they may be extremely time-dependent and during a phase transition, assuming a constant C_p is not justified. Subsequent heating and cooling cycles show no further significant irreversibility within the accuracy of the measurements, which is expected because without further quenching steps the samples that were heated once retain only one reversible phase transition at 400 °C from a long periodically trigonal phase to the cubic HT phase. The density of the samples does not change significantly among the differently ordered variants of the compounds after the phase transitions. Both quenched and HT phases are cubic so that anisotropy effects should not affect the measurements; they may, however, occur in the trigonal phase in the same way they do in "classical" TAGS materials.

dx.doi.org/10.1021/ic5010243 | Inorg. Chem. 2014, 53, 7722−7729

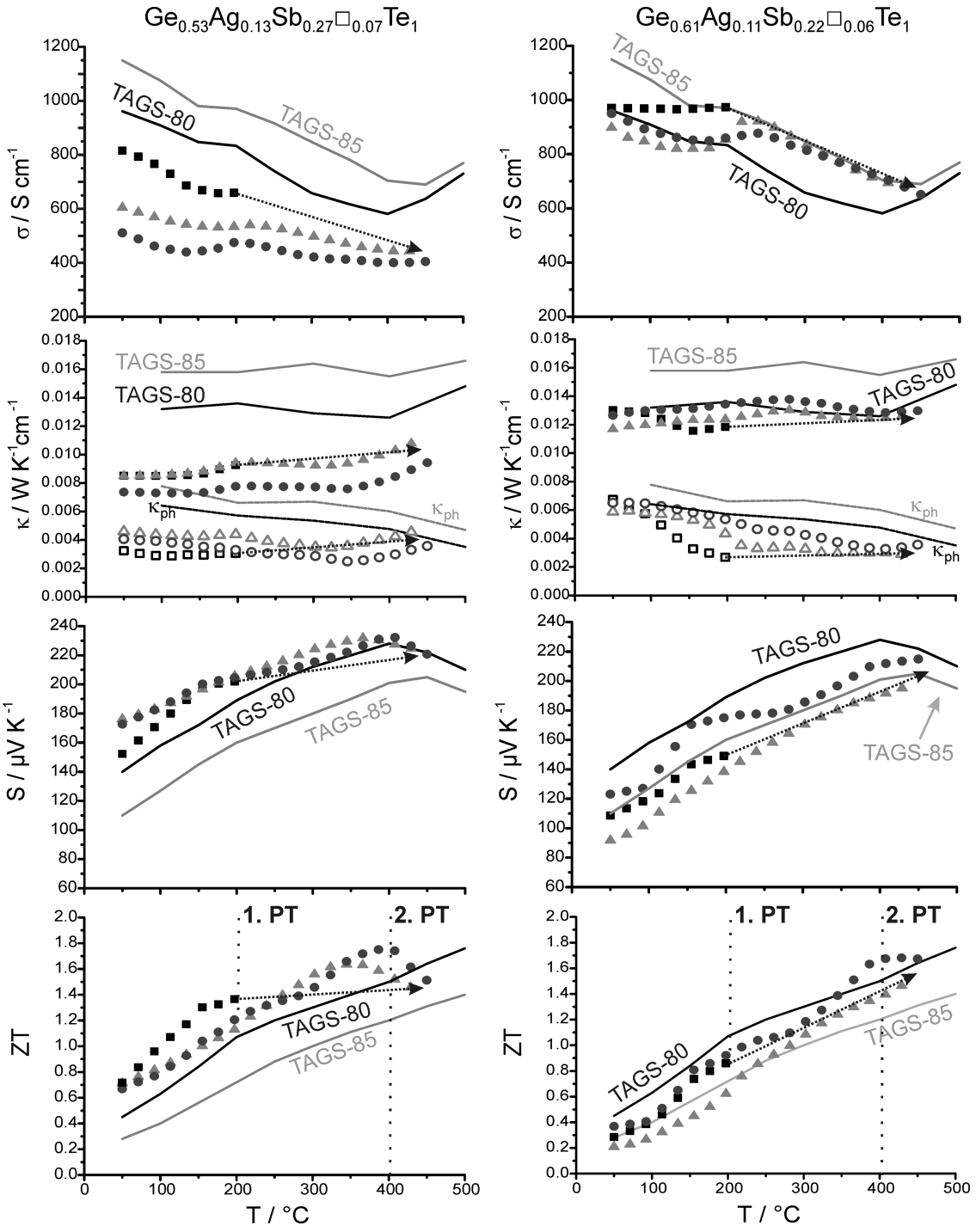

Figure 5. Electrical conductivity σ, thermal conductivity κ (phononic contribution κ_{ph} with empty symbols), Seebeck coefficient S, and ZT values (top to bottom: first heating cycle, black squares; first cooling cycle, gray triangles; second heating cycle, dark gray circles, some slight offsets are within the error limits of the methods and result from remounting the samples) of $Ge_{0.53}Ag_{0.13}Sb_{0.27}\square_{0.07}Te_1$ (left) and $Ge_{0.61}Ag_{0.11}Sb_{0.22}\square_{0.06}Te_1$ (right) in comparison to TAGS-80 (black line) and TAGS-85 (gray line) as taken from ref 17 with recalculated κ_{ph} (marked by black/gray κ_{ph} for TAGS-80 and TAGS-85, respectively). In the ZT plot the phase transition temperatures (1. and 2. PT as discussed in the text) are marked by dotted lines; the values between 200 and 450 °C during the first heating cycle are not shown (the arrows just indicate further heating) because they are strongly affected by slow irreversible phase transitions (see discussion).

Below 200 °C, $Ge_{0.53}Ag_{0.13}Sb_{0.27}\square_{0.07}Te_1$ outperforms both TAGS-80 and TAGS-85 and other recently reported high-performance TAGS materials.[17,24] The properties of the isotropic nanostructured modification at the beginning of the first heating cycle are remarkable although they could only be exploited if the samples are never heated over 200 °C. The ZT value of 1.3 at 160 °C, i.e., below any phase transition temperature, is higher than that of TAGS-80 (or any other TAGS sample) at the same temperature. While σ and S of $Ge_{0.53}Ag_{0.13}Sb_{0.27}\square_{0.07}Te_1$ are comparable to those of TAGS-80, the high ZT value is due to the low thermal conductivity; especially, its phononic contribution (calculated with a Lorenz

dx.doi.org/10.1021/ic5010243 | Inorg. Chem. 2014, 53, 7722−7729

number as reported for TAGS materials with vacancies of 2×10^{-8} V^2 K^{-2})[24] is significantly reduced in comparison to TAGS materials without vacancies. However, these favorable values may additionally be associated with a change in the carrier concentration and mobility, which is another consequence of the adjusted Ag/Sb ratio.[26] For the consecutive cooling and heating cycle, the ZT values are in good accordance with the values recently published for TAGS materials with Ag/Sb rations deviating from 1.[24,26]

For $Ge_{0.61}Ag_{0.11}Sb_{0.22}\square_{0.06}Te_1$, consecutive heating and cooling cycles vary less than for the sample with the slightly higher cation vacancy concentration. The lattice contribution to the thermal conductivity is again lower than the one observed for conventional TAGS materials, but not as low as for $Ge_{0.53}Ag_{0.13}Sb_{0.27}\square_{0.07}Te_1$, and increases when the nanostructure vanishes. σ and S are comparable to TAGS-85, while κ corresponds to TAGS-80. This leads to slightly higher ZT values than those of TAGS-85, but it does not outperform TAGS-80 and other high-performance TAGS materials. These observations clearly show the huge influence of minor changes of the vacancy concentration.

CONCLUSION

The best conventional vacancy-free TAGS materials, i.e., TAGS-80 and TAGS-85, differ only little concerning their chemical composition: by 6 atom % for Ge and 3 atom % for Ag and Sb. Thus, there is a rather limited compositional range for further optimization. We focus on two homogeneous compounds with optimized Ag/Sb ratio, involving the presence of cation vacancies. According to the present investigation, the enhanced thermoelectric properties result from these more or less short-range ordered cation vacancies. They might act as phonon scattering centers as indicated by the significant reduction of the phononic contribution to the thermal conductivity while the good electrical properties remain almost unchanged in comparison to conventional vacancy-free TAGS materials. The cation vacancy concentration also plays a crucial role concerning the structural chemistry of TAGS materials. For high cation vacancy concentrations, the structures are in remarkable contrast to those reported for conventional TAGS materials.[11−14,17] Both $Ge_{0.53}Ag_{0.13}Sb_{0.27}\square_{0.07}Te_1$ and $Ge_{0.61}Ag_{0.11}Sb_{0.22}\square_{0.06}Te_1$ can be quenched to form metastable compounds with a rock-salt-type average structure and layer-like short-range ordered vacancies. In contrast, lower vacancy concentrations as in $Ge_{0.77}Ag_{0.07}Sb_{0.13}\square_{0.03}Te_1$ lead to a TAGS-like α-GeTe-type structure which implies that cation ordering effects do not play an important role.

Quenched, nanostructured compounds with high cation vacancy concentrations exhibit two phase transitions. An irreversible transition leads from a (pseudo)cubic "parquet-like" multidomain nanostructure to a long-periodically ordered trigonal one and a second, reversible transition to a cubic rock-salt-type HT phase. Although the partial irreversibility and phase transitions in general may be viewed as drawbacks concerning thermal cycling, nanostructured $Ge_{0.53}Ag_{0.13}Sb_{0.27}\square_{0.07}Te_1$ may be applied far below any phase transition temperature, where it exhibits a ZT value of 1.3 at 160 °C. Annealed samples, or those heated over 200 °C just once, exhibit only one reversible phase transition. Their thermoelectric properties still differ from conventional vacancy-free TAGS, as do their structures. These findings are in good accordance with the values recently published for high-performance TAGS materials.[23,24,26] Our results clearly illustrate how the structural chemistry of this multinary system can be significantly changed even when the composition is varied only slightly as this involved a much more pronounced relative change of the vacancy concentration. In addition to altered charge carrier concentrations, different short- or long-range ordering variants of the cation vacancies significantly influence the thermoelectric properties and are one reason for the high performance of TAGS material with a Ag/Sb ratio differing from 1. It remains an open question if conventional TAGS materials, despite the fact that their chemical formulas formally suggest vacancy-free structures, may also exhibit a certain amount of vacancies that contribute to their performance.

ASSOCIATED CONTENT

Supporting Information

Table containing the SEM-EDX results, further HRTEM images with their corresponding SAED patterns and/or Fourier transforms as well as the Rietveld fit with a structure image and a table containing the atom positions, occupancy factors, and displacement factors for the stable modification of $Ge_{0.53}Ag_{0.13}Sb_{0.27}\square_{0.07}Te_1$. Crystallographic data in CIF format. This material is available free of charge via the Internet at http://pubs.acs.org.

AUTHOR INFORMATION

Corresponding Author

*E-mail: oliver.oeckler@gmx.de. Fax: (+49)341-97-36299.

Notes

The authors declare no competing financial interest.

ACKNOWLEDGMENTS

We thank Thomas Miller and Christian Minke (LMU Munich) for the temperature-dependent powder diffraction experiments and for SEM-EDX analyses, respectively. We are grateful to Prof. Dr. W. Schnick (LMU Munich) for the generous support of this work. Furthermore, we thank Fivos Drymiotis (California Institute of Technology) for help with the thermoelectric measurements. This investigation was funded by the Deutsche Forschungsgemeinschaft (Grant OE530/1−2) and the Studienstiftung des deutschen Volkes (scholarship for T.S.).

REFERENCES

(1) Sootsman, J. R.; Chung, D. Y.; Kanatzidis, M. G. *Angew. Chem., Int. Ed.* **2009**, *48*, 8616−8639.
(2) Wood, C. *Rep. Prog. Phys.* **1988**, *51*, 459−539.
(3) Morelli, D. T.; Jovovic, V.; Heremans, J. P. *Phys. Rev. Lett.* **2008**, *101*, 035901.
(4) Schröder, T.; Rosenthal, T.; Souchay, D.; Petermayer, C.; Grott, S.; Scheidt, E.-W.; Gold, C.; Scherer, W.; Oeckler, O. *J. Solid State Chem.* **2013**, *206*, 20−26.
(5) Mohanraman, R.; Sankar, R.; Boopathi, K. M.; Chou, F.-C.; Chu, C.-W.; Lee, C.-H.; Chen, Y.-Y. *J. Mater. Chem. A* **2014**, *2*, 2839−2844.
(6) Hsu, K. F.; Loo, S.; Guo, F.; Chen, W.; Dyck, J. S.; Uher, C.; Hogan, T.; Polychroniadis, E. K.; Kanatzidis, M. G. *Science* **2004**, *303*, 818−821.
(7) Zeier, W. G.; Pei, Y. Z.; Pomrehn, G.; Day, T.; Heinz, N.; Heinrich, C. P.; Snyder, G. J.; Tremel, W. *J. Am. Chem. Soc.* **2013**, *135*, 726−732.
(8) Yusufu, A.; Kurosaki, K.; Ohishi, Y.; Muta, H.; Yamanaka, S. *Jpn. J. Appl. Phys.* **2013**, *52*, 081801.

(9) Plirdpring, T.; Kurosaki, K.; Kosuaga, A.; Day, T.; Firdosy, S.; Ravi, V.; Snyder, G. J.; Harnwunggmoung, A.; Sugahara, T.; Ohishi, Y.; Muta, H.; Yamanaka, S. *Adv. Mater.* **2012**, *24*, 3622−3626.
(10) Liu, R.; Xi, L.; Liu, H.; Shi, X.; Zhang, W.; Chen, L. *Chem. Commun.* **2012**, *48*, 3818−3820.
(11) Cook, B. A.; Kramer, M. J.; Wei, X.; Harringa, J. L.; Levin, E. M. *J. Appl. Phys.* **2007**, *101*, 053715.
(12) Plachkova, S. K. *Phys. Status Solidi A* **1984**, *83*, 349−355.
(13) Yang, S. H.; Zhu, T. J.; Sun, T.; Zhang, S. N.; Zhao, X. B.; He, J. *Nanotechnology* **2008**, *19*, 245707.
(14) Rosi, F. D.; Dismukes, J. P.; Hockings, E. F. *Electr. Eng.* **1960**, *79*, 450−459.
(15) Klemm, W.; Frischmuth, G. *Z. Anorg. Allg. Chem.* **1934**, *218*, 249−251.
(16) Goldak, J.; Barrett, C. S.; Innes, D.; Youdelis, W. *J. Chem. Phys.* **1966**, *44*, 3323−3325.
(17) Davidow, J.; Gelbstein, Y. *J. Electron. Mater.* **2013**, *42*, 1542−1549.
(18) Shi, X.; Salvador, J. R.; Yang, J.; Wang, H. *Sci. Adv. Mater.* **2011**, *3*, 667−671.
(19) Schröder, T.; Schwarzmüller, S.; Stiewe, C.; de Boor, J.; Hölzel, M.; Oeckler, O. *Inorg. Chem.* **2013**, *52*, 11288−11294.
(20) Schröder, T.; Rosenthal, T.; Giesbrecht, N.; Maier, S.; Scheidt, E.-W.; Scherer, W.; Snyder, G. J.; Schnick, W.; Oeckler, O. *J. Mater. Chem. A* **2014**, *2*, 6384−6395.
(21) Levin, E. M.; Cook, B. A.; Harringa, J. L.; Bud'ko, S. L.; Venkatasubramanian, R.; Schmidt-Rohr, K. *Adv. Funct. Mater.* **2011**, *21*, 441−447.
(22) Levin, E. M.; Bud'ko, S. L.; Schmidt-Rohr, K. *Adv. Funct. Mater.* **2012**, *22*, 2766−2774.
(23) Christakudis, G. C.; Plachkova, S. K.; Shelimova, L. E.; Avilov, E. S. *Phys. Status Solidi A* **1991**, *128*, 465−471.
(24) Zhu, T.; Gao, H.; Chen, Y.; Zhao, X. B. *J. Mater. Chem. A* **2014**, *2*, 3251−3256.
(25) Chen, Y.; He, B.; Zhu, T. J.; Zhao, X. B. *J. Phys. D: Appl. Phys.* **2012**, *45*, 115302.
(26) Chen, Y.; Jaworski, C. M.; Gao, Y. B.; Wang, H.; Zhu, T. J.; Snyder, G. J.; Heremans, J. P.; Zhao, X. B. *New J. Phys.* **2014**, *16*, 013057.
(27) Schneider, M. N.; Rosenthal, T.; Stiewe, C.; Oeckler, O. *Z. Kristallogr.* **2010**, *225*, 463−470.
(28) Rosenthal, T.; Schneider, M. N.; Stiewe, C.; Döblinger, M.; Oeckler, O. *Chem. Mater.* **2011**, *23*, 4349−4356.
(29) *TOPAS-Academic, V. 4.1*; Coelho Software: Brisbane, Australia, 2007.
(30) *WINXPOW, v2.12*; Stoe & Cie GmbH: Darmstadt, Germany, 2005.
(31) *DigitalMicrograph, 3.6.1*; Gatan Software: Pleasanton, CA, 1999.
(32) Stadelmann, P. A. *Ultramicroscopy* **1987**, *21*, 131−145.
(33) *ESVision, 4.0.164*; Emispec Systems Inc.: Tempe, AZ, 1994−2002.
(34) Borup, K. A.; Toberer, E. S.; Zoltan, L. D.; Nakatsukasa, G.; Errico, M.; Fleurial, J. P.; Iversen, B. B.; Snyder, G. J. *Rev. Sci. Instrum.* **2012**, *83*, 123902.
(35) van der Pauw, L. J. *Philips Res. Rep.* **1958**, *13*, 1−9.
(36) Wang, H.; Porter, W. D.; Böttner, H.; König, J.; Chen, L.; Bai, S.; Tritt, T. M.; Mayolet, A.; Senawiratne, J.; Smith, C.; Harris, F.; Gilbert, P.; Sharp, J. W.; Lo, J.; Kleinke, H.; Kiss, L. *J. Electron. Mater.* **2013**, *42*, 1073−1084.
(37) Iwanaga, S.; Toberer, E. S.; LaLonde, A.; Snyder, G. J. *Rev. Sci. Instrum.* **2011**, *82*, 063905.
(38) Rosenthal, T.; Urban, P.; Nimmrich, K.; Schenk, L.; de Boor, J.; Stiewe, C.; Oeckler, O. *Chem. Mater.* **2014**, *26*, 2567−2578.
(39) Schneider, M. N.; Oeckler, O. *Z. Anorg. Allg. Chem.* **2008**, *634*, 2557−2561.